ACS APPLIED MATERIALS & INTERFACES

Research Article

www.acsami.org

Smart Floor with Integrated Triboelectric Nanogenerator As Energy Harvester and Motion Sensor

Chuan He,[†,‡] Weijun Zhu,[§,∥] Baodong Chen,[†,‡] Liang Xu,[†,‡] Tao Jiang,[†,‡] Chang Bao Han,[†,‡] Guang Qin Gu,[†,‡,⊥] Dichen Li,[§,∥] and Zhong Lin Wang*[,†,‡,#]

[†]Beijing Institute of Nanoenergy and Nanosystems, Chinese Academy of Sciences, Beijing 100083, China

[‡]CAS Center for Excellence in Nanoscience, National Center for Nanoscience and Technology (NCNST), Beijing 100190, China

[§]State Key Laboratory of Manufacturing Systems Engineering and [∥]Collaborative Innovation Center of High-End Manufacturing Equipment, Xi'an Jiaotong University, Xi'an 710049, Shaanxi China

[⊥]University of Chinese Academy of Sciences, Beijing 100049, China

[#]School of Materials Science and Engineering, Georgia Institute of Technology, Atlanta, Georgia 30332, United States

Supporting Information

ABSTRACT: A smart floor is demonstrated by integrating a square-frame triboelectric nanogenerator (SF-TENG) into a standard wood floor. The smart floor has two working modes based on two pairs of triboelectric materials: one is purposely chosen polytetrafluoroethylene films and aluminum (Al) balls, and the other is the floor itself and the objects that can be triboelectrically charged, such as basketball, shoe soles, and Scotch tape, etc. Utilizing the Al balls enclosed inside shallow boxes, the smart floor is capable of harvesting vibrational energy and, hence, provides a nonintrusive way to detect sudden falls in elderly people. In addition, when the basketball is bounced repeatedly on the floor, the average output voltage and current are 364 ± 43 V and 9 ± 1 μA, respectively, and 87 serially connected light-emitting diodes can be lit up simultaneously. Furthermore, the friction between the triboelectrically chargeable objects and the floor can also induce an alternating current output in the external circuit without the vibration of the Al balls. Normal human footsteps on the floor produce a voltage of 238 ± 17 V and a current of 2.4 ± 0.3 μA. Therefore, this work presents a smart floor with built-in SF-TENG without compromising the flexibility and stability of the standard wood floor and also demonstrates a way to harvest ambient energy solely by using conventional triboelectric materials in our daily life.

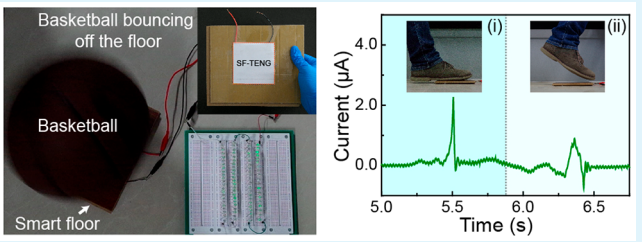

KEYWORDS: *smart floor, triboelectric nanogenerator, Al balls, energy harvester, motion sensor*

INTRODUCTION

With further advances in miniaturization, electronic devices can benefit from energy harvesters to eliminate the necessity for battery replacement, hence making the system maintenance-free.[1−6] Ever since its discovery, triboelectric nanogenerator (TENG) has become a strong candidate among energy-harvesting devices.[5−9] In general, it employs two dissimilar triboelectric materials, preferably of opposite tribo-polarity, to generate electrostatic charges on their respective surfaces. Then, through periodic motion, such as contacting and separating[10−12] or sliding,[13,14] between the materials, a potential difference can be created periodically between two electrodes attached to the materials, hence generating an alternating current (AC) output in the external circuit. On the basis of the triboelectric effect and electrostatic induction, TENGs of various structures have been utilized to harvest low-frequency mechanical energy, such as human motion,[15−18] wind,[19,20] vibration,[10,21] ultrasonic wave energy,[22] and water waves.[23] Because the TENG is sensitive to mechanical agitations, it has also been widely applied as pressure and touch sensors,[24−26] motion sensors,[7,27] and acceleration sensors.[28] However, triboelectric effect generally requires intimate contact between the materials that might results in material abrasion and frictional heating, thus affecting the long-term performance of the TENGs. To circumvent these problems, TENGs that operated in noncontact mode have been developed by separating triboelectric materials from electrodes spatially.[29−31] In this regard, triboelectric materials are first charged through triboelectrification. Because these charges can retain on their respective surfaces for a long time, the periodic motion of the materials afterward in a noncontact way between two electrodes produces an AC output as a result of electrostatic induction.

Mostly, materials in everyday life, such as clothes, paper, and glass, are triboelectrically chargeable; thus, the spatial separation of the triboelectric material and the electrodes provides a way to harvest ambient energy using the materials in our daily life. In this article, we demonstrate a smart floor with integrated

Received: June 13, 2017
Accepted: July 14, 2017
Published: July 14, 2017

DOI: 10.1021/acsami.7b08526
ACS Appl. Mater. Interfaces XXXX, XXX, XXX−XXX

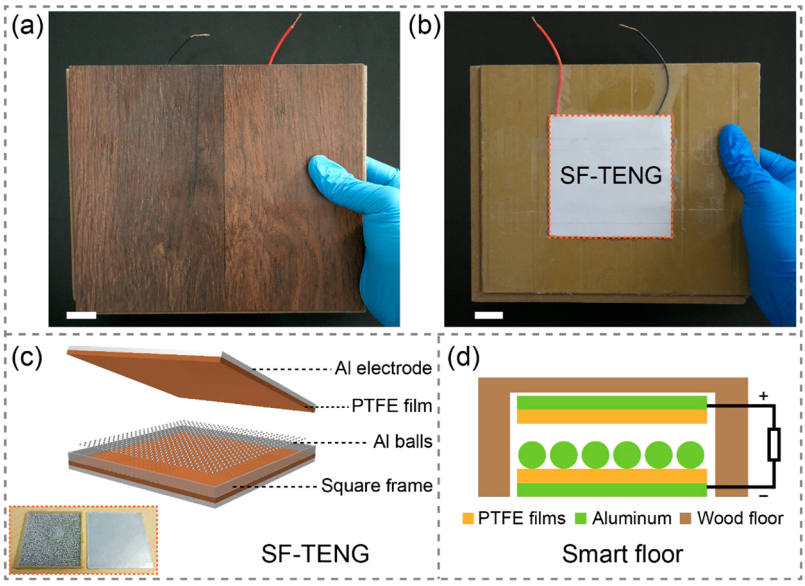

Figure 1. Photograph of the (a) front side and (b) back side of the smart floor, where the SF-TENG is installed. The scale bars in panels a and b are 20 mm; (c) schematic illustration of the SF-TENG. The inset is the photograph of the SF-TENG; (d) the cross-sectional view of the smart floor.

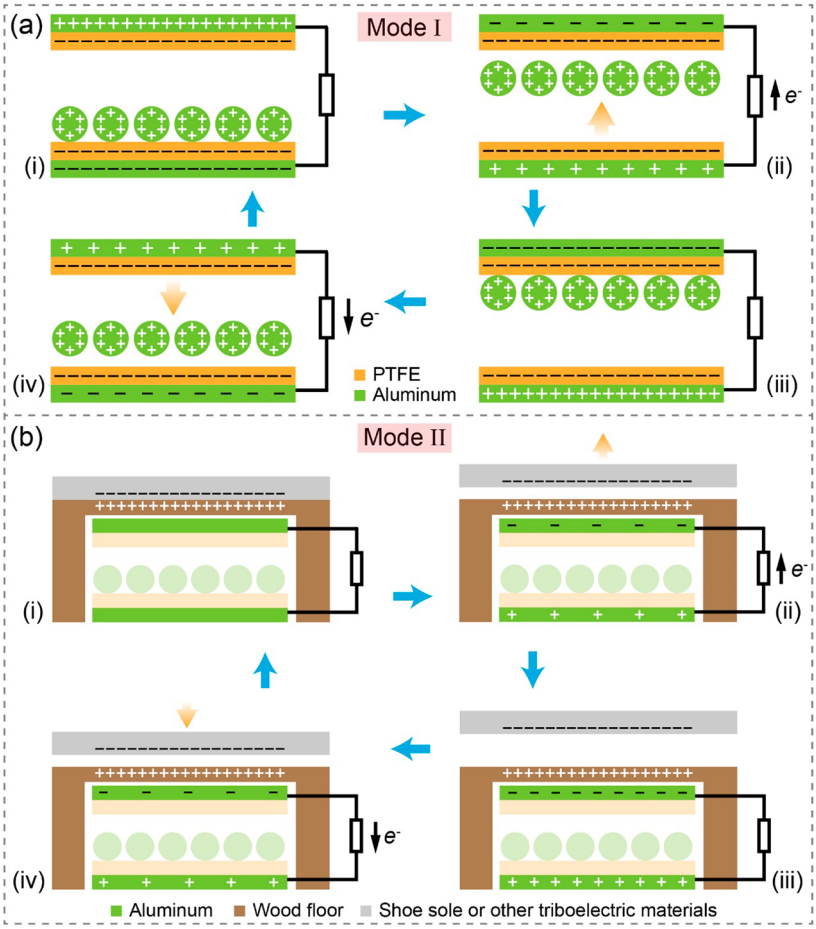

Figure 2. Working principle of the SF-TENG. (a) Mode I; (b) Mode II.

square-frame TENG (SF-TENG) as energy harvester and motion sensor. Here, the smart floor, which is made of wood, can operate not only using purposely chosen polytetrafluoroethylene (PTFE) films and aluminum (Al) balls but also using the floor itself and the objects that come into contact with it (for example, basketballs, shoe soles, Scotch tape, etc.) as triboelectric materials. The SF-TENG embedded has only a thickness of 6 mm and encloses Al balls with a diameter of 1 mm; thus, the SF-TENG can be integrated into the standard wood floor without compromising the flexibility and stability.

DOI: 10.1021/acsami.7b08526
ACS Appl. Mater. Interfaces XXXX, XXX, XXX−XXX

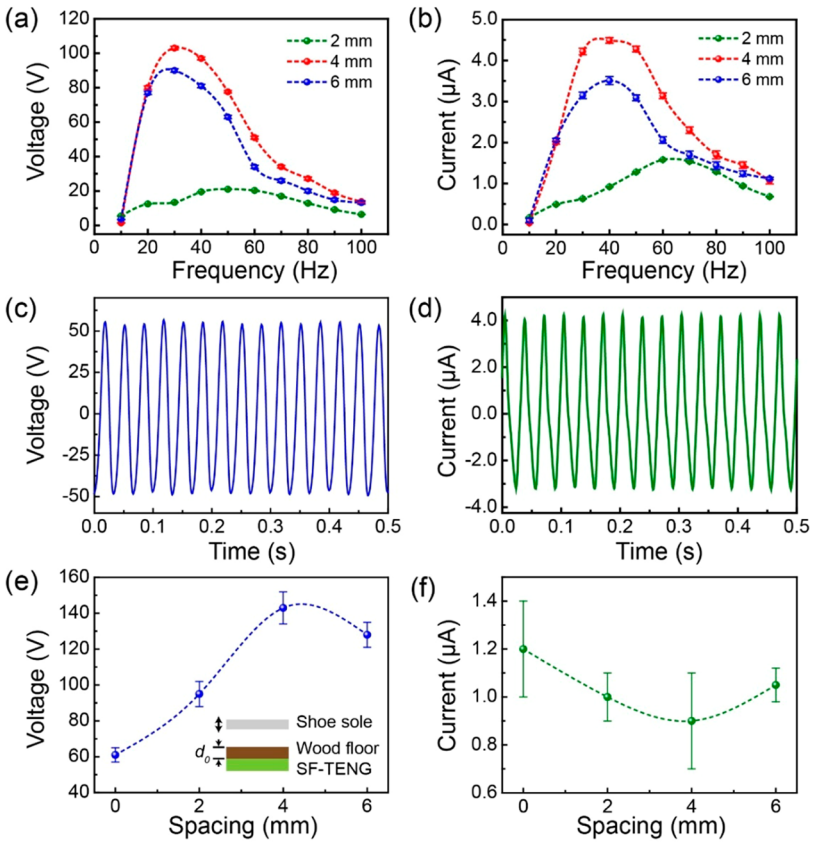

Figure 3. (a) Open-circuit voltage (V_{OC}) and (b) short-circuit current (I_{SC}) of the SF-TENG with different spacings (2, 4, and 6 mm) as a function of vibrational frequency. (c) Open-circuit voltage at vibrational frequency of 30 Hz. (d) Short-circuit current at a vibrational frequency of 30 Hz. The (e) V_{OC} and (f) I_{SC} of the integrated SF-TENG produced by consecutive steps as a function of the spacing between the top and the bottom PTFE films.

Utilizing the Al balls inside, the smart floor can be used to sense sudden falls in elderly people, and moreover, it can harvest energy from various vibrational sources, such as jumping of athletes or the bouncing of basketballs on a basketball court. As for indoor human activities (take walking, for example), because shoe soles and wood are both triboelectric materials, the footsteps on the floor will generate static charges on both surfaces. Thus, the energy of human walking can be harvested or sensed without the vibration of the Al balls.

RESULTS AND DISCUSSION

Panels a and b of Figure 1 show the photographs of the front and back side of the smart floor, respectively, where the SF-TENG is integrated into a commercial wood floor. The wood floor is chosen because it is one of the most common floor choices. It can be seen that the wood floor is carved from the back side, so that the SF-TENG can be fitted into it. Due to the low thickness of the SF-TENG, the wood floor still maintains its hardness afterward. The structural design of the SF-TENG is illustrated in Figure 1c. The SF-TENG has a 3D-printed square frame with a side length of 83 mm and an inner side length of 80 mm, which is fabricated by stereolithography (SL). Each side of the square frame is covered by a layer of PTFE film placed on top of an Al plate. Inside the frame are the Al balls with a diameter of 1 mm. The Al balls act as electropositive triboelectric materials, while the PTFE film is an electronegative layer according to the triboelectric series.[32] The Al plates on the top and bottom sides act as both the electrode and the protecting layer. Figure 1d depicts the cross-sectional view of the smart floor, where the top and bottom electrodes are connected to the positive and negative probe, respectively, through our experiments. The detailed fabrication process of the SF-TENG is presented in the Experimental section.

The working principle of the SF-TENG is depicted in Figure 2. There are two working modes of the SF-TENG. In Mode I, as shown in Figure 2a, when the TENG is subjected to an external force or vibration, the Al balls inside will oscillate between the top and bottom plates, hence driving the electrons through the external circuit. When the Al balls get in contact with the PTFE films, the electrons will be injected from the Al balls to the PTFE films as a result of the triboelectric effect.[32] Thus, the total amount of positive triboelectric charges on the Al balls should be the same with the negative triboelectric charges on the PTFE films. As illustrated in Figure 2a-i, when the Al balls stay at the bottom, negative charges are attracted to the bottom electrode, leaving the same amount of positive charges on the top Al electrode. As the Al balls approach the top plate, the electrons on the bottom electrode will transfer to the top one because the top electrode has a higher potential (see Figure 2a-ii). All the electrons are transferred to the top electrode once the Al balls reach the top PTFE film (see Figure 2a-iii). Then as the Al balls move toward the bottom electrode, the electrons are driven in the reverse direction through the external circuit (see Figure 2a-iv). At last, when the Al balls return to the bottom, a full cycle is completed (see Figure 2a-i).

Besides harvesting vibrational energy using the Al balls, the smart floor is also capable of harnessing energy of the objects that get in contact with the floor by taking advantage of the fact

DOI: 10.1021/acsami.7b08526
ACS Appl. Mater. Interfaces XXXX, XXX, XXX−XXX

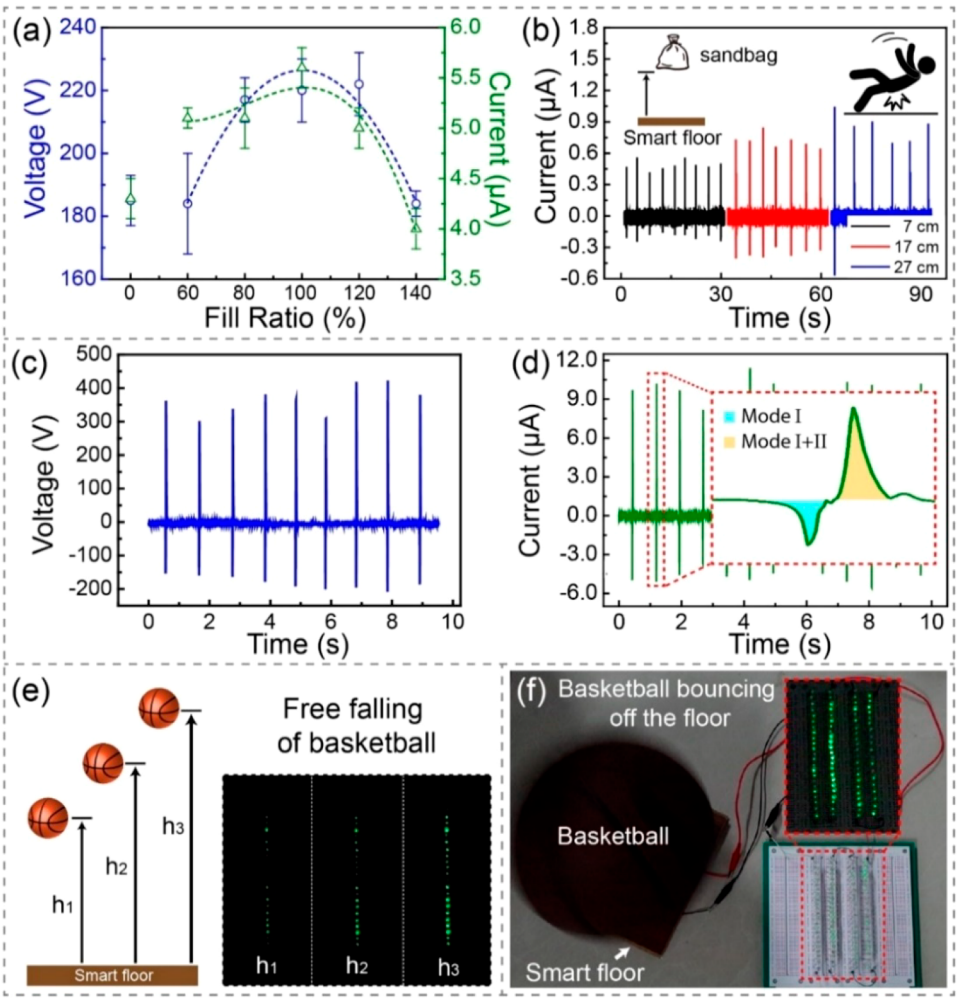

Figure 4. (a) Open-circuit voltage and short-circuit current of the SF-TENG with different fill ratios (0%, 60%, 80%, 100%, 120%, and 140%); (b) demonstration of the SF-TENG as fall detection sensor; (c) the V_{OC} and (d) I_{SC} of the SF-TENG as the basketball bounces on the floor repeatedly. (e) A row of LEDs being lit up by free-falling basketball at different height (h_1 = 40 cm, h_2 = 80 cm, and h_3 = 120 cm). (f) Demonstration of the smart floor as energy harvester: four rows of LEDs (~87 LEDs) being lit up when the basketball bounces off the floor.

that the floor and the objects are normally triboelectric materials. Thus, the smart floor provides an alternative method of harnessing the energy from human activities, such as walking and dancing, without requiring any deformation or vibration of the floor. The mechanism of this working mode (Mode II) is illustrated in Figure 2b, where the human walking is used as an example. It is noted that the footsteps applied throughout the measurements are gentle so that no Al balls vibrate; thus, for clarification, we only take two Al electrodes of the SF-TENG into consideration. Initially, as indicated in Figure 2b-i, when the shoe sole is fully in contact with the smart floor as a person steps on it, the electrons transfer from the surface of the floor into the shoe sole (depending on their triboelectric polarity) due to the triboelectric effect. Once the shoe sole is taken off the floor (see Figure 2b-ii), the top electrode, which is closer to the floor surface, has a higher potential than the bottom one; thus, electrons flow to the top electrode on the external circuit. As the shoe sole gets further away, the electrostatic equilibrium is reached (see Figure 2b-iii). Conversely, as the shoe sole approaches the floor, the electrons are driven back to the bottom electrode (see Figure 2b-iv). When the shoe sole is in full contact with the floor again, the reverse flow of the electrons ceases (see Figure 2b-i).

To determine the optimum thickness of the SF-TENG, i.e., the optimum spacing between the top and bottom PFTE films, the electrical performance of the SF-TENG with different spacings are evaluated under two working modes. The electrical performance of the SF-TENG in Mode I was first evaluated using an electrodynamic shaker (Labworks Inc.), in which sinusoidal vibrations with a fixed amplitude and tunable frequency are produced. By attaching to the shaker, the output dependence of the SF-TENGs on vibrational frequency was measured with a fill ratio of 60%. The fill ratio is defined as the area ratio of close-packed Al balls to the PTFE film. The open-circuit voltage (V_{OC}) and short-circuit current (I_{SC}) of the SF-TENG over the vibrational frequency (10−100 Hz) are plotted in panels a and b of Figure 3, respectively. Here, 3 different heights (2, 4, and 6 mm) of the square frame, i.e., the spacings between the top and bottom PTFE films, is used in the SF-TENGs. From panels a and b of Figure 3, it is clear that the SF-TENGs of different distance (d) values are all capable of harvesting the vibrational energy over the measured frequency. When the spacing equals to 2 mm, the V_{OC} and I_{SC} of the SF-TENG peaked at 50 and 60 Hz, respectively; at the frequency of 60 Hz, the V_{OC} and I_{SC} produced are 20.3 ± 0.1 V and 1.58 ± 0.01 μA, respectively. As the spacing increases, both the V_{OC}

DOI: 10.1021/acsami.7b08526
ACS Appl. Mater. Interfaces XXXX, XXX, XXX−XXX

and I_{SC} increase dramatically over the vibrational frequency. In the meantime, the peak values of the V_{OC} and I_{SC} are shifted to 30 and 40 Hz, respectively. At the frequency of 30 Hz, the V_{OC} of the SF-TENGs with a spacing of 4 and 6 mm are 103 ± 1 and 90 ± 1 V, respectively, while at the frequency of 40 Hz, the I_{SC} are 4.49 ± 0.07 and 3.5 ± 0.1 μA, respectively. We can see that the SF-TENG with the spacing of 4 mm delivers the best output performance in the measured frequency range. The reason can be attributed to the fact that when the spacing equals to 2 mm, as shown in Figure 2a-i, there is a relatively strong Coulomb force between the Al balls and top electrode, which results in a small potential difference between the top and bottom electrodes. As the spacing increases, the Coulomb force decreases, and thus, the potential difference increases. In the meantime, the increasing spacing also leads to a smaller contact force and a decreased contact area as the Al balls vibrate, thus yielding a decreased potential difference between the electrodes. It can be seen from the results that the spacing of 4 mm reached a balance between the two effects. Panels c and d of Figure 3 show the V_{OC} and I_{SC} of the SF-TENG with a spacing of 4 mm at the frequency of 30 Hz, respectively, where both output signals are quasi-sinusoidal. Panels e and f of Figure 3 present the V_{OC} and I_{SC} of the SF-TENG as a function of the spacing under Mode II. Here, the measurements were taken by consecutively steps on and off the smart floor, as indicated in the inset of Figure 3e. The distance, d_0, between the surface of the wood floor and SF-TENG is ∼6 mm. Because Mode II does not require the participation of the Al balls, the fill ratio of the SF-TENG used here is 0%, and the spacing used is 0, 2, 4, and 6 mm. We can see that the V_{OC} generated by consecutive steps peaks at 4 mm, while the I_{SC} produced stayed consistent at different spacings. These results indicate that the SF-TENG is capable of working under two modes independently. Taking both Mode I and Mode II into consideration, the SF-TENG with a spacing of 4 mm exhibits the best electrical performance.

Except for the spacing between the PTFE films, the fill ratio is another key factor that affect the performance of the SF-TENG. By the integration of the SF-TENG with a spacing of 4 mm into the wood floor (see Figure 1d), the relationship between the electrical output and the fill ratio of the integrated SF-TENG is investigated systematically. The measurements were taken by dropping a basketball at the height of 80 cm, which serves as a vibrational source. In this situation, the surfaces of the basketball and the floor are triboelectrically charged as the basketball gets in contact with the floor. Thus, each time the basketball hits the floor, the integrated SF-TENG produces a transient AC current flow in the external circuit. Figure 4a shows the magnitude of the positive peaks of the V_{OC} and I_{SC} with different fill ratios: 0%, 60%, 80%, 100%, 120%, and 140%. To begin with, when there are no Al balls inside, i.e., the fill ratio is 0%, the SF-TENG is able to generate a voltage of 185 ± 8 V and a current of 4.3 ± 0.2 μA under Mode II. When the Al balls are added, the kinetic energy of the basketball can be transferred to the Al balls and causes them to vibrate, hence converting to the electrical energy under Mode I. As the fill ratio increases (that is, the number of Al balls placed into the SF-TENG increases), more charges are transferred between the Al balls and PTFE films; thus, there is an increase in the electrical output, as shown in Figure 4a. The maximum output occurs at the fill ratio of 100%, where the V_{OC} and I_{SC} generated is 220 ± 10 V and 5.6 ± 0.2 μA, respectively. Due to the small thickness of the SF-TENG, as the fill ratio keeps increasing, the distance between the Al balls and PTFE films decreases, and hence, the potential difference between the two electrodes also decreases. Therefore, as the Al balls vibrate, the electrical output of SF-TENG decreases. Compared to the fill ratio of 0%, the SF-TENGs with the fill ratio of 80%, 100%, and 120% have a higher electrical output. These results indicate that the SF-TENGs with the Al balls enclosed can be operated in two working modes simultaneously, and the maximum output occurs at the fill ratio of 100%. Therefore, the SF-TENG with a spacing of 4 mm and the fill ratio of 100% is chosen for the following experiments and demonstrations.

Due to its stiffness and easy maintenance, the wood floor has been widely installed in homes or sport courts; for example, the wood floor has always been the traditional choice for basketball courts. When integrated with the SF-TENG, a smart floor can serve as a fall-detection sensor for elderly people at home, and moreover, the smart floor can harness the energy from various vibration sources, such as bouncing balls or the jumping of an athlete on such courts. The fall-detection sensor, as a part of the medical alert system, is designed for detecting falls in elderly people who live alone. Commonly, fall detection sensors rely on wearable technology (for example, a wristband-type TENG) has been proposed to detect the fall of the elderly.[33] However, long-term wear of the sensors might be intrusive and uncomfortable for the users, especially for the ones who stay at home. Here, the capability of the smart floor as a fall detection sensor is demonstrated using a 1 kg sandbag that free falls from different heights. Considering the fact that most of the falls might happen at slippery spots, where no surface charges exist, the measurements were taken by slightly wetting the surface of the smart floor, so that the SF-TENG only works under Mode I. Figure 4b shows the I_{SC} produced by the integrated SF-TENG as a 1 kg sandbag free-falls on the smart floor. The heights used are 7, 17, and 27 cm. As can be seen in Figure 4b, each time the sandbag hits the smart floor, a current pulse is generated. It is noted that the pulse consists of a positive peak and a negative peak that follows afterward. This pulse profile reflects a full cycle of vibration, as indicated in Figure 2a. As the height increases from 7 to 27 cm, the peak value of the current increases from 0.49 ± 0.05 to 0.8 ± 0.1 μA. Clearly, under Mode I, the falling events can be detected; hence the smart floor provides a nonintrusive method for detecting the fall of elderly people at home.

Besides sensing the unintentional falls of elderly people, a smart floor as an energy harvester is demonstrated by bouncing the basketball repeatedly on the floor. The electrical outputs of the SF-TENG produced are illustrated in panels c and d of Figure 4, where the average output voltage and current are 364 ± 43 V and 9 ± 1 μA, respectively. The inset of Figure 4d depicts an enlarged view of the current pulse, which consists of a negative and a positive peak. The negative peak arises as the basketball approaches the floor (Mode II, Figure 2b-iv). Once the basketball hits the floor, the kinetic energy of the basketball transfers to the Al balls, hence producing a transient positive current (Mode I, Figure 2a-ii). Furthermore, the basketball bouncing off the floor also generates a positive current (Mode II, Figure 2b-ii). As discussed previously, the positive peak generated by the vibration of the Al balls follows a negative peak (Mode I, Figure 2a-iv). The reasons for not observing this negative peak are twofold: first, the electrical output produced under Mode II is dominant over that under Mode I, as shown in Figure 4a, and second, the duration of positive peak generated under Mode II is approximately the same as duration

DOI: 10.1021/acsami.7b08526
ACS Appl. Mater. Interfaces XXXX, XXX, XXX−XXX

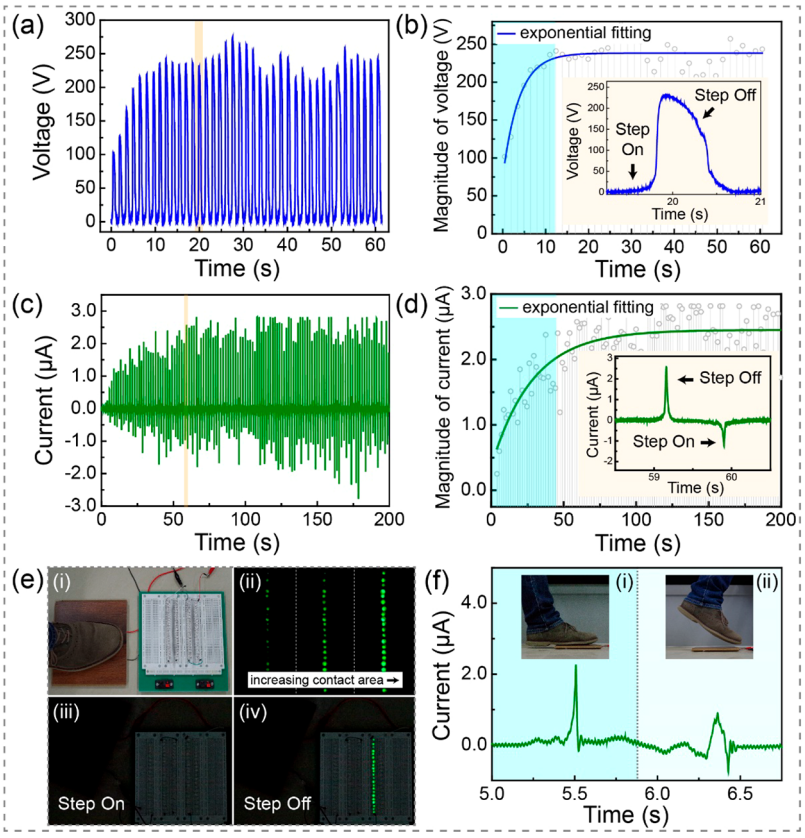

Figure 5. (a) Open-circuit voltage of the integrated SF-TENG produced by consecutive footsteps; (b) magnitude of the V_{OC} and the exponential fitting. The inset shows the enlarged view of voltage peak highlighted in panel a; (c) short-circuit current of the integrated SF-TENG produced by consecutive footsteps; (d) magnitude of the I_{SC} and the exponential fitting. The inset shows the enlarged view of current peak highlighted in panel c; (e) photograph of a row of serially connected LEDs being lit up as the foot step off the floor; (f) the I_{SC} of the footstep during walking.

of the current pulse generated in one cycle under Mode I (includes both positive and negative peaks), where the duration is around 0.016 s. The capability of the SF-TENG as a power source is demonstrated in panels e and f of Figure 4. Figure 4e shows the free-falling of the basketball from different heights (h_1 = 40 cm, h_2 = 80 cm, and h_3 = 120 cm) to light up a row of serially connected light emitting diodes (LEDs). We can see that as the height increases, the intensity of the light also increases. As we bounce the ball on the floor repeatedly, each bounce can light up 4 rows of serially connected LEDs (~87 LEDs), as demonstrated in Figure 4(f). The inset are the LEDs being lit up in a dimmer environment for better illustration (Video S1).

Generally, indoor human activities, such as walking, do not have enough kinetic energy to cause the Al balls vibrate inside the integrated SF-TENG, hence the smart floor in these situations works only under Mode II. The V_{OC} generated by consecutive footsteps (no vibration of the Al balls involved) is shown in Figure 5a, while the magnitude of the V_{OC} and the exponential fitting are depicted in Figure 5b. It can be seen that the first footstep on the floor generates a voltage of ~100 V. With consecutive footsteps, the magnitude of the V_{OC} first increases and then remains stable afterward. At the beginning, the increasing voltage is attributed to the accumulation of charges on the contact surfaces with each footstep; when the surfaces are saturated with the charges, the magnitude of the V_{OC} generated is 238 ± 17 V. The inset of Figure 5b shows the highlighted region in Figure 5a. When the foot steps on the floor, as indicated in Figure 2b-i, there is no potential difference between the top and bottom electrode; once the foot steps off the floor, the top electrode has a higher potential, and hence, a positive voltage peak is produced. The I_{SC} generated by the SF-TENG shows a similar pattern in Figure 5c, and the magnitude of the I_{SC} generated as the foot steps off of the floor and the exponential fitting are depicted in Figure 5d, where the current saturates at 2.4 ± 0.3 μA. The highlighted part in Figure 5c is enlarged in the inset of Figure 5d. As the foot steps on the floor, a negative peak is generated, and the step off of the floor produces a positive peak, which is in accordance with the analysis in Figure 2b.

Figure 5e demonstrates the smart floor as the energy harvester and motion sensor under Mode II. A photograph of the smart floor that directly connected to the LEDs is shown in Figure 5e-i. We can see that as the foot steps off the floor, a row of serially connected LEDs can be lit up (Video S2), and the intensity of the LEDs increases with increasing contact area between the surfaces, as illustrated in Figure 5e-ii–iv. Additionally, as a person walks by the smart floor, the I_{SC} produced has two positive peaks, as shown in Figure 5f. The first peak (panel i) arises as the foot steps on the floor, while shortly afterward, another positive current (panel ii) is generated as the foot is taken off the floor. Different from consecutive footsteps on the wood floor, here it is shown that as the foot steps on the wood floor, a positive peak is generated, indicating the net negative charges appear on the shoe sole before it gets in contact with the smart floor. Besides the shoe soles, we also tested other triboelectric materials that get in contact with the smart floor. For example, the V_{OC} and I_{SC} of

DOI: 10.1021/acsami.7b08526
ACS Appl. Mater. Interfaces XXXX, XXX, XXX−XXX

the SF-TENG as the bare hand taps on and off the smart floor are illustrated in panels a and b of Figure S1, respectively. Moreover, for the rolling of a roll of Scotch tape (width: ~50 mm) over the smart floor, the V_{OC} and I_{SC} of the SF-TENG are shown in panels a and b of Figure S2, respectively. We can see that as the speed of the tape increases, the duration of the generated signal decreases. Hence, the smart floor can sense not only the motion but also the speed of the rolling tape.

We have presented a single unit of the smart floor with integrated SF-TENG as energy harvester and motion sensor. With the optimized size and number of the integrated SF-TENGs, the smart floor equipped at a sport court, such as basketball and volleyball courts, can not only harvest the energy of the players and the bouncing balls but also could be used to sense whether the ball is out of bounds, especially near the boundaries. When the array of the integrated SF-TENGs is equipped at home, a smart floor is capable of sensing the movement of a person and thus can serve as an automatic switch for lighting, ventilation, and air conditioning, etc. or as an invisible sensor in the surveillance system for detecting unusual behavior, such as thefts and break-ins. Thus, smart floors may play an important role in next-generation home-automation systems.

CONCLUSIONS

In conclusion, we demonstrate a smart floor with built-in SF-TENG for energy-harvesting and sensing purposes. The SF-TENG with a thickness of 6 mm encloses Al balls with a diameter of 1 mm and is integrated into the commercial wood floor. The smart floor has two different working modes. Utilizing the Al balls enclosed, the values of I_{SC} produced by the SF-TENG as a 1 kg sandbag free-falls on the smart floor from different heights are measured. As the height increases from 7 to 27 cm, the peak value of the current increases from 0.49 ± 0.05 to 0.8 ± 0.1 μA. Thus, the smart floor can be used to sense the sudden fall of an elderly in a nonintrusive way. The smart floor can also harvest energy from various vibrational sources. When the basketball was bounced repeatedly on the floor, the average output voltage and current are 364 ± 43 V and 9 ± 1 μA, respectively, and each bounce can light up 4 rows of serially connected LEDs (~87 LEDs). Furthermore, the smart floor can capture the energy or sense the motion of the triboelectrically chargeable objects, such as shoe soles, bare hands, and rolls of Scotch tape. Take walking for example, normal footsteps produce a voltage of 238 ± 17 V and a current of 2.4 ± 0.3 μA. This work demonstrates a way to harvest ambient energy solely using the triboelectric materials in our daily life.

EXPERIMENTAL SECTION

The SF-TENG consists of a square frame, Al balls, and two PTFE films on the Al plates. The square frame has a side length of 83 mm, while the inner side length is 80 mm. The square frame is fabricated using epoxy acrylate by stereolithography, which has a resolution of ±0.1 mm. The thickness of the SF-TENG is 6 mm, while the height of the frame, i.e., the spacing between the PTFE films, is 4 mm. Inside the frame is filled with the Al balls with a diameter of 1 mm. On each side of the square frame is a layer of PTFE film placed on top of the Al plate. The thickness of the PTFE films is 80 μm, while the Al plate has a thickness of 1 mm. The standard wood floor used has a size of 195 × 167 mm and a thickness of 12 mm. All of the electrical measurements of the SF-TENG were performed using the Keithley 6514 system electrometer (except for the open-circuit voltage of the SF-TENG as the basketball bounces off the floor; see Figure 4c). A function generator (Stanford Research Systems DS345) and a linear power amplifier (Labworks PA-141) were used to produce the sinusoidal oscillations. A vibration shaker (Labworks ET-126B-4) was used to simulate mechanical vibration.

ASSOCIATED CONTENT

Supporting Information

The Supporting Information is available free of charge on the ACS Publications website at DOI: 10.1021/acsami.7b08526.

Figures showing open-circuit voltages and short-circuit currents of the SF-TENG. (PDF)

A video showing four rows of serially connected LEDs being lit up as the basketball bounces on the smart floor repeatedly. (AVI)

A video showing a row of serially connected LEDs being lit up as a foot steps on and off the smart floor. (AVI)

AUTHOR INFORMATION

Corresponding Author

*E-mail: zlwang@gatech.edu.

ORCID

Zhong Lin Wang: 0000-0002-5530-0380

Funding

Support from the "Thousand Talents" program for the pioneer researcher and his innovation team, the National Key R & D Project from Minister of Science and Technology (2016YFA0202704), the National Natural Science Foundation of China (grant nos. 51432005, 51608039, 5151101243, 51561145021, and 51505457), the China Postdoctoral Science Foundation (grant no. 2015M581041), and the Natural Science Foundation of Beijing, China (grant no. 4154090) is appreciated.

Notes

The authors declare no competing financial interest.

ABBREVIATIONS

PTEF, polytetrafluoroethylene
AC, alternating current
TENG, triboelectric nanogenerator
SF-TENG, square-frame triboelectric nanogenerator
SL, stereolithography

REFERENCES

(1) Bell, L. E. Cooling, Heating, Generating Power, and Recovering Waste Heat with Thermoelectric Systems. *Science* **2008**, *321*, 1457−1461.

(2) Wang, Z. L.; Song, J. Piezoelectric Nanogenerators Based on Zinc Oxide Nanowire Arrays. *Science* **2006**, *312*, 242−246.

(3) Zhang, Y.; Yang, Y.; Gu, Y.; Yan, X.; Liao, Q.; Li, P.; Zhang, Z.; Wang, Z. Performance and Service Behavior in 1-D Nanostructured Energy Conversion Devices. *Nano Energy* **2015**, *14*, 30−48.

(4) Zhang, G.; Liao, Q.; Ma, M.; Zhang, Z.; Si, H.; Liu, S.; Zheng, X.; Ding, Y.; Zhang, Y. A Rationally Designed Output Current Measurement Procedure and Comprehensive Understanding of the Output Characteristics for Piezoelectric Nanogenerators. *Nano Energy* **2016**, *30*, 180−186.

(5) Fan, F.-R.; Tian, Z.-Q.; Wang, Z. L. Flexible Triboelectric Generator. *Nano Energy* **2012**, *1*, 328−334.

(6) Wang, Z. L.; Chen, J.; Lin, L. Progress in Triboelectric Nanogenerators as a New Energy Technology and Self-Powered Sensors. *Energy Environ. Sci.* **2015**, *8*, 2250−2282.

DOI: 10.1021/acsami.7b08526
ACS Appl. Mater. Interfaces XXXX, XXX, XXX−XXX

(7) Zhang, Q.; Liang, Q.; Liao, Q.; Yi, F.; Zheng, X.; Ma, M.; Gao, F.; Zhang, Y. Service Behavior of Multifunctional Triboelectric Nanogenerators. *Adv. Mater.* **2017**, *29*, 1606703.
(8) Lee, S. H.; Jeong, C. K.; Hwang, G.-T.; Lee, K. J. Self-Powered Flexible Inorganic Electronic System. *Nano Energy* **2015**, *14*, 111−125.
(9) Liu, G.; Guo, H.; Chen, L.; Wang, X.; Wei, D.; Hu, C. Double-Induced-Mode Integrated Triboelectric Nanogenerator Based on Spring Steel to Maximize Space Utilization. *Nano Res.* **2016**, *9*, 3355−3363.
(10) Chen, J.; Zhu, G.; Yang, W.; Jing, Q.; Bai, P.; Yang, Y.; Hou, T.-C.; Wang, Z. L. Harmonic-Resonator-Based Triboelectric Nanogenerator as a Sustainable Power Source and a Self-Powered Active Vibration Sensor. *Adv. Mater.* **2013**, *25*, 6094−6099.
(11) Zhong, J.; Zhong, Q.; Fan, F.; Zhang, Y.; Wang, S.; Hu, B.; Wang, Z. L.; Zhou, J. Finger Typing Driven Triboelectric Nanogenerator and Its Use for Instantaneously Lighting up Leds. *Nano Energy* **2013**, *2*, 491−497.
(12) Wang, H. S.; Jeong, C. K.; Seo, M.-H.; Joe, D. J.; Han, J. H.; Yoon, J.-B.; Lee, K. J. Performance-Enhanced Triboelectric Nanogenerator Enabled by Wafer-Scale Nanogrates of Multistep Pattern Downscaling. *Nano Energy* **2017**, *35*, 415−423.
(13) Du, W.; Han, X.; Lin, L.; Chen, M.; Li, X.; Pan, C.; Wang, Z. L. A Three Dimensional Multi-Layered Sliding Triboelectric Nanogenerator. *Adv. Energy Mater.* **2014**, *4*, 1301592.
(14) Jing, Q.; Zhu, G.; Bai, P.; Xie, Y.; Chen, J.; Han, R. P. S.; Wang, Z. L. Case-Encapsulated Triboelectric Nanogenerator for Harvesting Energy from Reciprocating Sliding Motion. *ACS Nano* **2014**, *8*, 3836−3842.
(15) Wang, J.; Li, S.; Yi, F.; Zi, Y.; Lin, J.; Wang, X.; Xu, Y.; Wang, Z. L. Sustainably Powering Wearable Electronics Solely by Biomechanical Energy. *Nat. Commun.* **2016**, *7*, 12744.
(16) Li, S.; Wang, J.; Peng, W.; Lin, L.; Zi, Y.; Wang, S.; Zhang, G.; Wang, Z. L. Sustainable Energy Source for Wearable Electronics Based on Multilayer Elastomeric Triboelectric Nanogenerators. *Adv. Energy Mater.* **2017**, *7*, 1602832.
(17) Yang, W.; Chen, J.; Zhu, G.; Yang, J.; Bai, P.; Su, Y.; Jing, Q.; Cao, X.; Wang, Z. L. Harvesting Energy from the Natural Vibration of Human Walking. *ACS Nano* **2013**, *7*, 11317−11324.
(18) Li, X. H.; Han, C. B.; Zhang, L. M.; Wang, Z. L. Cylindrical Spiral Triboelectric Nanogenerator. *Nano Res.* **2015**, *8*, 3197−3204.
(19) Bae, J.; Lee, J.; Kim, S.; Ha, J.; Lee, B.-S.; Park, Y.; Choong, C.; Kim, J.-B.; Wang, Z. L.; Kim, H.-Y.; Park, J.-J.; Chung, U. I. Flutter-Driven Triboelectrification for Harvesting Wind Energy. *Nat. Commun.* **2014**, *5*, 4929.
(20) Xie, Y.; Wang, S.; Lin, L.; Jing, Q.; Lin, Z.-H.; Niu, S.; Wu, Z.; Wang, Z. L. Rotary Triboelectric Nanogenerator Based on a Hybridized Mechanism for Harvesting Wind Energy. *ACS Nano* **2013**, *7*, 7119−7125.
(21) Yang, J.; Chen, J.; Yang, Y.; Zhang, H.; Yang, W.; Bai, P.; Su, Y.; Wang, Z. L. Broadband Vibrational Energy Harvesting Based on a Triboelectric Nanogenerator. *Adv. Energy Mater.* **2014**, *4*, 1301322.
(22) Xi, Y.; Wang, J.; Zi, Y.; Li, X.; Han, C.; Cao, X.; Hu, C.; Wang, Z. High Efficient Harvesting of Underwater Ultrasonic Wave Energy by Triboelectric Nanogenerator. *Nano Energy* **2017**, *38*, 101−108.
(23) Wang, Z. L. New Wave Power. *Nature* **2017**, *542*, 159−160.
(24) Lin, L.; Xie, Y.; Wang, S.; Wu, W.; Niu, S.; Wen, X.; Wang, Z. L. Triboelectric Active Sensor Array for Self-Powered Static and Dynamic Pressure Detection and Tactile Imaging. *ACS Nano* **2013**, *7*, 8266−8274.
(25) Meng, B.; Tang, W.; Too, Z.-h.; Zhang, X.; Han, M.; Liu, W.; Zhang, H. A Transparent Single-Friction-Surface Triboelectric Generator and Self-Powered Touch Sensor. *Energy Environ. Sci.* **2013**, *6*, 3235−3240.
(26) Ma, M.; Zhang, Z.; Liao, Q.; Yi, F.; Han, L.; Zhang, G.; Liu, S.; Liao, X.; Zhang, Y. Self-Powered Artificial Electronic Skin for High-Resolution Pressure Sensing. *Nano Energy* **2017**, *32*, 389−396.
(27) Jing, Q.; Xie, Y.; Zhu, G.; Han, R. P.; Wang, Z. L. Self-Powered Thin-Film Motion Vector Sensor. *Nat. Commun.* **2015**, *6*, 8031.
(28) Pang, Y. K.; Li, X. H.; Chen, M. X.; Han, C. B.; Zhang, C.; Wang, Z. L. Triboelectric Nanogenerators as a Self-Powered 3d Acceleration Sensor. *ACS Appl. Mater. Interfaces* **2015**, *7*, 19076−19082.
(29) Lin, L.; Wang, S.; Niu, S.; Liu, C.; Xie, Y.; Wang, Z. L. Noncontact Free-Rotating Disk Triboelectric Nanogenerator as a Sustainable Energy Harvester and Self-Powered Mechanical Sensor. *ACS Appl. Mater. Interfaces* **2014**, *6*, 3031−3038.
(30) Li, S.; Wang, S.; Zi, Y.; Wen, Z.; Lin, L.; Zhang, G.; Wang, Z. L. Largely Improving the Robustness and Lifetime of Triboelectric Nanogenerators through Automatic Transition between Contact and Noncontact Working States. *ACS Nano* **2015**, *9*, 7479−7487.
(31) Wang, S.; Xie, Y.; Niu, S.; Lin, L.; Wang, Z. L. Freestanding Triboelectric-Layer-Based Nanogenerators for Harvesting Energy from a Moving Object or Human Motion in Contact and Non-Contact Modes. *Adv. Mater.* **2014**, *26*, 2818−2824.
(32) Wang, Z. L. Triboelectric Nanogenerators as New Energy Technology for Self-Powered Systems and as Active Mechanical and Chemical Sensors. *ACS Nano* **2013**, *7*, 9533−9557.
(33) Jung, S.; Hong, S.; Kim, J.; Lee, S.; Hyeon, T.; Lee, M.; Kim, D.-H. Wearable Fall Detector Using Integrated Sensors and Energy Devices. *Sci. Rep.* **2015**, *5*, 17081.

DOI: 10.1021/acsami.7b08526
ACS Appl. Mater. Interfaces XXXX, XXX, XXX−XXX